Progress In Electromagnetics Research C, Vol. 125, 253–264, 2022

A Low-Profile Dual-Band Circularly Polarized Antenna with Wide 3-dB Axial Ratio Beamwidth for Beidou Applications

Wen Wang, Jingchun Zhai, Gengliang Chen, and Zhuopeng Wang*

Abstract—A thin dual band circularly polarized (CP) patch antenna with a wide 3-dB axial ratio beamwidth (ARBW) is presented for BeiDou Navigation System (BDS) application. The CP radiation is achieved using simple stacked square patches for dual band radiation in the BDS B1 band (1561 ± 2 MHz) and B3 band (1268 ± 10 MHz). A 'string moon' type branch extension technique is proposed to enhance the ARBW and axial ratio bandwidth in both operating bands. Loading 30° gap-type annular parasitic metal strips (APMS) further improves the ARBW in both operating bands. The experimental results show that the impedance bandwidth of the antenna is 6.3% (1.25–1.33 GHz) and 4.5% (1.52–1.59 GHz), and the axial ratio bandwidth is 1.6% (1.26–1.28 GHz) and 1.2% (1.55–1.57 GHz), respectively. In addition, the 3-dB ARBWs in the $\varphi = 0°$ and $\varphi = 90°$ planes are 185° and 184° at 1.268 GHz, respectively; and 222° and 211° at 1.561 GHz, respectively. The simulated results are in good agreement with the measured ones.

1. INTRODUCTION

Global navigation satellite system has been widely used in many fields such as navigation, position fixing, public security, and surveillance. China's self-developed navigation satellite system is named BeiDou Navigation Satellite System (BDS) and provides positioning services for the whole world. For high-precision positioning, the required circularly polarized (CP) antenna should have the characteristics of right-handed circularly polarized (RHCP) radiation, good gain, wide ARBW, and compact size, among which the size and ARBW of the antenna are more important than impedance bandwidth and gain to provide a wide coverage angle and suppress multipath effect [1]. As an example, a CP antenna with a width of 3-dB ARBW greater than 120 is commonly used. This can ensure that the navigation satellite can effectively receive signals at any altitude [2, 3].

Generally speaking, spiral antennas [4, 5], improved rotary antennas [6], and microstrip antennas [7–14] can achieve wide 3-dB ARBW. Because microstrip antennas have the advantages of compactness, light weight, and low profile, they become the first choice for design compared to spiral wire antennas and modified rotating antennas. Yet, having a narrow 3-dB ARBW is the biggest disadvantage of the traditional CP microstrip antenna (CPMA). In recent years, in order to extend the 3-dB ARBW of CPMA, many researchers have proposed many new methods, such as replacing the two-dimensional plane with a three-dimensional ground plane [7, 9], using the aperture of the antenna [11–13], the loading of additional parasitic radiation progenitor [10, 19], and two pairs of parallel dipoles spaced in the square profile [3]. Nevertheless, the highly CP antenna profiles with three-dimensional ground planes [7–9] and additional radiating elements with complex geometries [10, 19] may cause manufacturing difficulties. The proposed antenna in [3] shows an undesired bi-directional radiation pattern. In [11], a hanging construction of decreased effective permittivity for determining the area of radiation is presented;

Received 25 September 2022, Accepted 14 October 2022, Scheduled 25 October 2022
* Corresponding author: Zhuopeng Wang (wzhuopeng1@sdust.edu.cn).
The authors are with the College of Electronic and Information Engineering, Shandong University of Science and Technology, Qingdao, China.

however, the properties of this antenna are very sensitive to the mounting error of the hanging heights. In [12, 13], a wide ARBW was presented using pin loading techniques. However, this structure is not applicable to antennas with electrically small size, and the ARBW becomes narrow when finite grounding is used. Moreover, these techniques are mainly studied for single band applications.

In the paper, a compact dual-band circularly polarized microstrip antenna is proposed to resonate at BDS B1 (1.561 GHz) and B3 (1.268 GHz). To enhance the 3-dB ARBW and axial ratio bandwidth, a 'string moon' type branch extension technique is proposed to achieve optimal overall antenna performance. Loading 30° gap-type APMS further enhances the 3-dB ARBW in both operating bands. Section 2 presents the detailed structure of the suggested antenna. In Sections 3 and 4, the effects of the suggested "string-moon" type branch extension technique and APMS are discussed, and the investigation of the parametric study is carried out. For demonstration purposes, a prototype of antenna is fabricated, and the actual performance is measured in Section 5. The proposed antenna is also compared with some previous dual-band CP antennas, and then conclusions are presented in Section 6. In particular, the proposed CP microstrip antenna has a compact dimension and good dual-band 3-dB ARBW performance.

2. ANTENNA STRUCTURE

The designed dual-band CP antenna is shown in Figure 1. It consists of two substrates (top and bottom substrates), two square radiating patches, which are upper patch and lower patch, and coaxial line feed. Each of the two substrates is an FR4 epoxy resin material with relative permittivity of 4.4, loss tangent of 0.02, and thicknesses of h_1 and h_2, respectively.

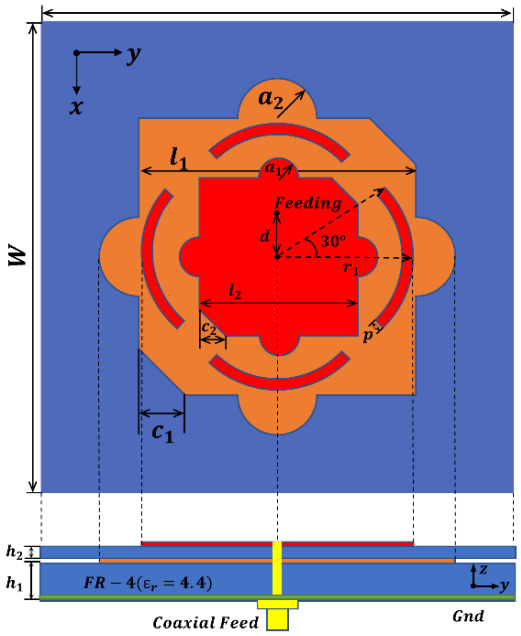

Figure 1. Geometric model of the proposed dual-band CPMA.

The antenna stacking patch is designed as a square patch. The square patch with side length l_2, as the main radiator of the upper band, is printed on the upper surface of the upper dielectric substrate. Moreover, the large square patch with side length l_1, as the lower frequency band main radiating body, is printed on the upper surface of the lower dielectric substrate. At the same time, two triangle cutting angles were introduced on the patch, and the edge length is c_2 and c_1, respectively. By this "degenerate separation unit", two radiation orthogonal polarizations of the degenerate mode is stimulated to achieve circular polarization. In order to improve the 3-dB ARBW and axial ratio

bandwidth of the two operating bands, a 'string-moon' type branch extension technique is proposed. The 'string-moon' type extension branches are extended outward with radius sizes a_1 and a_2 at the edge centers of the upper patch and lower patch, respectively. In addition, in order to further enhance the 3-dB ARBW, by loading 30° gap-type annular parasitic metal strips (APMS) around the upper patch, the radius of APMS is r_1, and the width is p. This structure can effectively increase the 3-dB ARBW. Table 1 shows the specific parameters of the suggested antenna. The profile height is only $0.016\lambda_0$, which shows that the antenna has a low-profile characteristic.

Table 1. Dimensions of the proposed antenna.

Parameters	W	l_2	c_2	l_1	c_1	a_1
Size (mm)	80	45.5	6	52.5	8	2
Parameters	a_2	r_1	p	h_1	h_2	
Size (mm)	4	30	3	3	1	

3. DESIGN PROCEDURE

The process of the evolution of the antenna is shown in Figure 2. Figures 3(a), (b), (c), (d) show the corresponding S_{11}, axial ratio bandwidth, and 3-dB ARBW when $\varphi = 0°$. First, a coaxially fed double-layer square patch is proposed, as shown in antenna 1 in Figure 2(a). In antenna 1, there are only two square patches of common coaxial feedback electricity. At this time, it is just a dual-band line polarized patch antenna, and the size L of the patch is derived from the following equation.

$$L = \frac{C}{2f_0\sqrt{\varepsilon_r}} \tag{1}$$

where ε_r is the relative permittivity of the medium, C the speed of light, and f_0 the B1 or B3 frequency point, respectively.

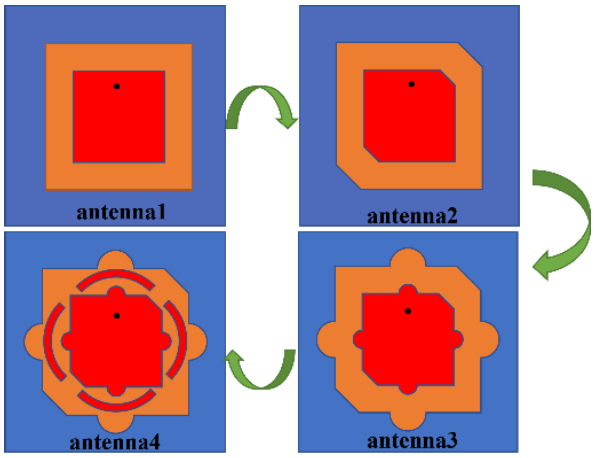

Figure 2. The process of the evolution of the antenna.

To obtain circular polarization characteristics, load different sizes of cutting corners on the diagonal line of two patches to obtain antenna 2. To expand the axial ratio bandwidth and 3-dB ARBW of the antenna, the proposed 'string moon' type extended branches are loaded at the center of the patch edges to form antenna 3. Finally, in antenna 4, 30° gap-type APMS is loaded around the upper patch. These antennas use the same substrate material, and the overall size is $80 \times 80 \times 4\,\text{mm}^3$.

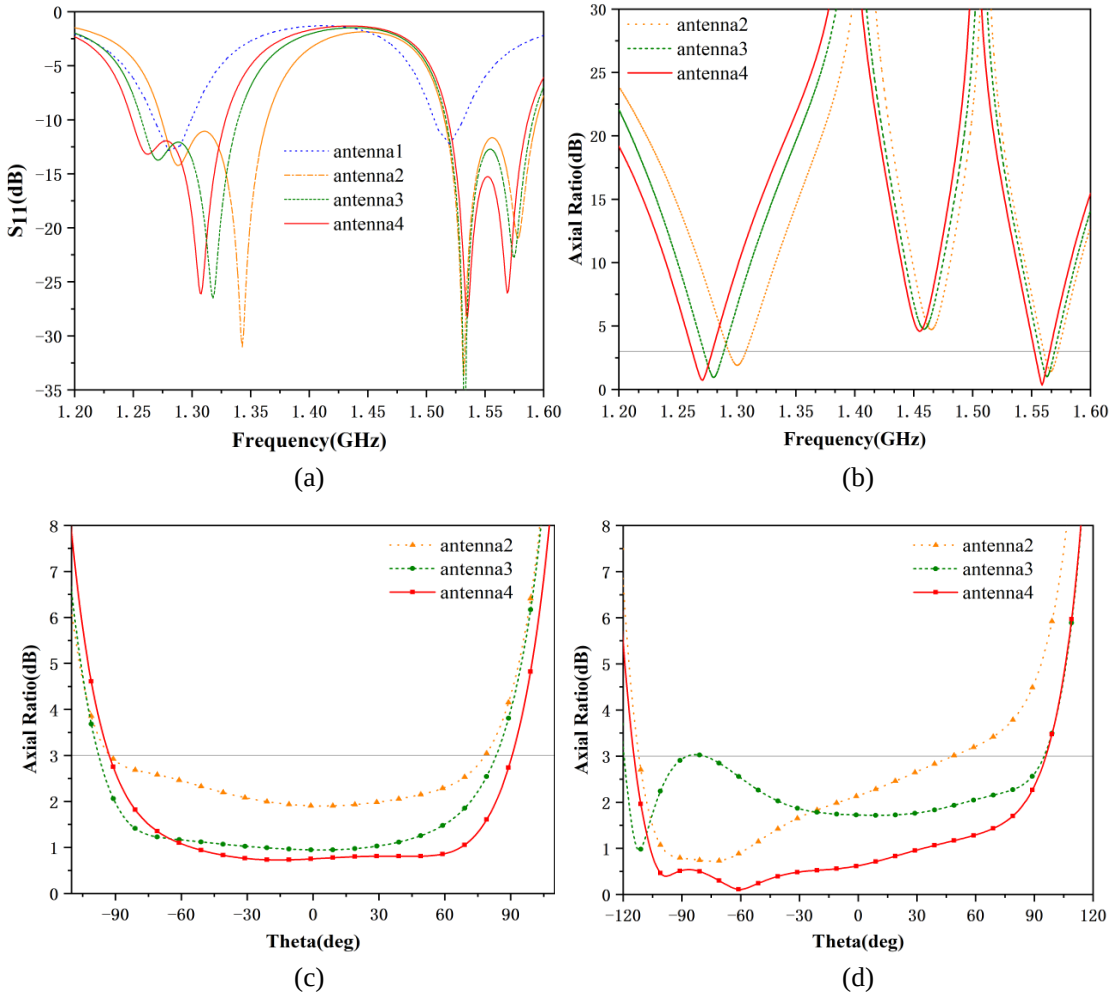

Figure 3. Performance comparison of each antenna during the evolution, (a) $|S_{11}|$, (b) Axial ratio, (c) 3 dB-ARBW at $\varphi = 0°$ plane in the lower band, (d) 3 dB-ARBW at $\varphi = 0°$ plane in the upper band.

Figure 3(a) shows the simulation results of the design $|S_{11}|$. As shown in the figure, the resonant frequency shifts upward from antenna 1 to antenna 2 under both bands. The reason for this phenomenon is that due to the cutting angle of the patch, the electrical length is reduced. At the same time, the lower-band resonance frequency from antenna 2 to antenna 3 decreases. The main reason is that the extension of the extended branch changes the current flow and affects the overall electrical length. Figure 3(b) shows the simulated AR of the antenna. As shown in the figure, the circular polarization performance is improved, and the axial ratio bandwidth is broadened by introducing a new structure.

On the XOZ plane, the 3 dB-ARBW of antennas 2, 3 and 4 at their respective frequency points are plotted in Figures 3(c) and 3(d). As shown in the figure, the 3-dB ARBW in the upper frequency band expands from 157° to 222° at the corresponding resonant frequencies from antenna 2 to antenna 4; the 3-dB ARBW in the lower frequency band expands from 168° to 185°.

3.1. Principle of Proposed CP Antenna

In this section, the operating principle of CP radiation generation from the proposed antenna is studied. The monofeed tangential circularly polarized microstrip antenna is based on the cavity model (CM) and works by two radiation orthogonal polarizations of the simple parallel modes (TM01 and TM10) [14]. To form a phase difference of 90° between TM01 and TM10 modes, a perturbation can be introduced at a tangent angle on the conductor patch to shift the resonant frequencies of both [14]. If the size of the

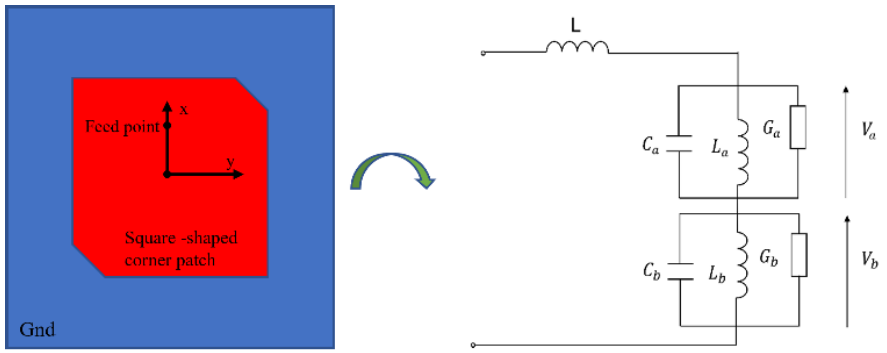

Figure 4. Equivalent circuit of tangential circularly polarized microstrip antenna.

tangent angle is selected appropriately for the working center frequency of the antenna, the equivalent phase of one mode will be 45° ahead, and the equivalent phase of the other mode will be 45° behind, so that circularly polarized radiation can be achieved at the working center frequency point of the antenna, and the axis ratio corresponding to this frequency point is minimum. Figure 4 shows the equivalent circuit of the tangential circularly polarized microstrip antenna. L is a small inductor caused by the higher-order mode; the resonant frequencies of the two parallel circuits are f_a and f_b, but the quality factor Q of both can be considered the same.

From Eq. (2), the circular polarization is obtained when the ratio of the voltage drop across the two radiation conductors is $\frac{V_b}{V_a} = \pm j$.

$$\frac{V_b}{V_a} = \frac{Z_b}{Z_a} = \frac{G_a}{G_b} \cdot \frac{1 + jQ_t\left(\frac{f}{f_a} - \frac{f_a}{f}\right)}{1 + jQ_t\left(\frac{f}{f_b} - \frac{f_b}{f}\right)} \approx \frac{\frac{f_a}{f} + jQ_t\left(1 - \frac{f_a^2}{f^2}\right)}{\frac{f_b}{f} + jQ_t\left(1 - \frac{f_b^2}{f^2}\right)} \tag{2}$$

Figure 5 shows the surface current distribution of the proposed antenna at $t = 0$, $t = T/8$, $T/4$ and $3T/8$, respectively, where t represents the periodicity of the electromagnetic wave in the B1 and B3 bands, respectively. It can be clearly seen that the currents rotate counterclockwise, indicating that

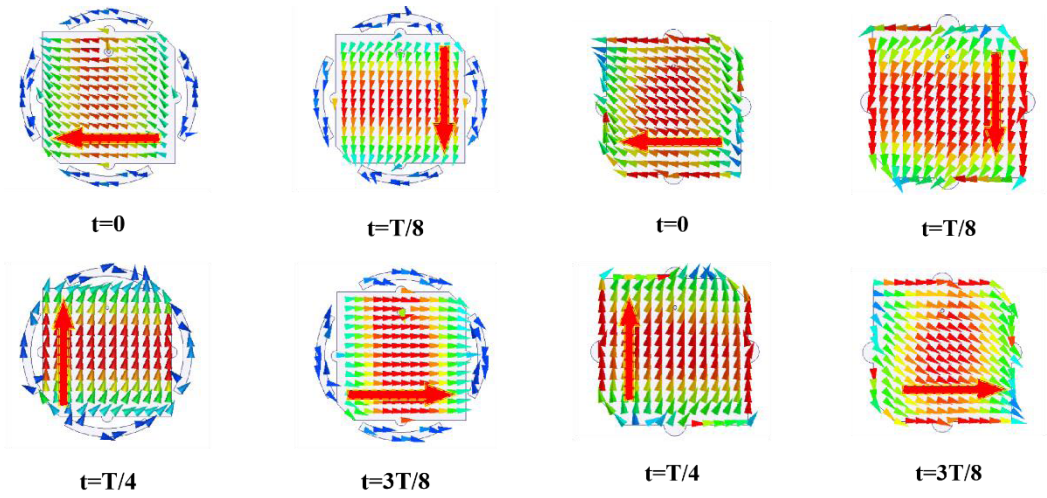

Figure 5. Simulation of current distribution at different time points (a) at 1.561 GHz, (b) at 1.268 GHz.

the polarization direction of the antenna is right circular polarization. The radiation pattern shown in Figure 13 can be further verified.

The variation of the magnetic field strength of antenna 2 and the proposed antenna 4 is shown in Figure 6. Because of the weak magnetic field, antenna 2 is limited to a narrow angle coverage of only 168° in the lower band and 161° in the upper band. For antenna 3, the loaded 'string moon' type extended branch is enhanced by 3 dB-ARBW. For the suggested CP antenna, the patch magnetic field is obviously stronger in the center due to the 30° gap-type APMS loaded around the upper patch, which has a Gaussian distribution along the feed axis [15]. The results show that it exhibits the widest 3-dB ARBW at two frequency bands $\varphi = 0°$ with 185° and 222°, respectively.

Figure 7 shows the axial ratio beamwidths of the two electric field components at B1 and B3 frequency points on different radiation surfaces, respectively. It can be clearly seen from the figure the

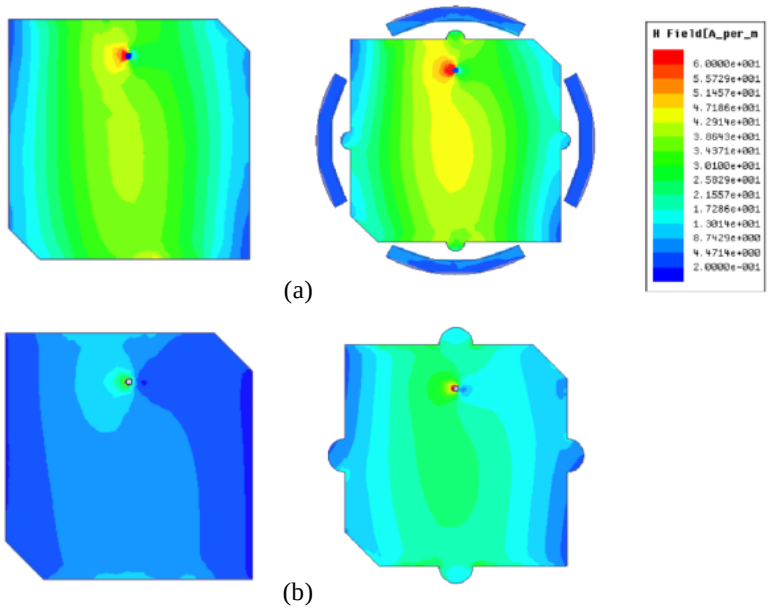

Figure 6. Surface magnetic field distribution of lower and upper patches of antenna 2 and antenna 4 (a) at 1.561 GHz, (b) at 1.268 GHz.

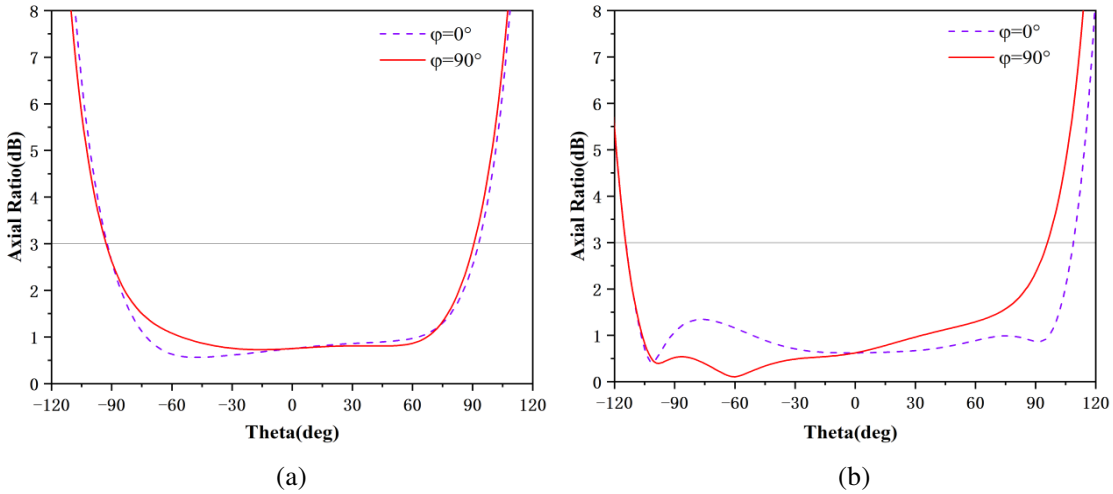

Figure 7. Dual-frequency 3-dB ARBW in two main planes (a) at 1.268 GHz, (b) at 1.561 GHz.

3-dB ARBWs 185° and 184° at 1.268 GHz in $\varphi = 0°$ and $\varphi = 90°$ planes, respectively, and the 3-dB ARBWs are 222° and 211° at 1.561 GHz, respectively. Therefore, the antenna is able to cover the entire upper hemispherical beam (facing the sky) with RHCP radiation.

4. PARAMETER ANALYSIS

The effect of various parameters on antenna radiation performance is investigated, especially the 3-dB ARBW. Due to the limited space of antenna parameters, only one geometric parameter is changed at a time, and the rest of the parameters are kept constant.

4.1. Effect of 'String Moon' Type Extended Branch Node Radius

In this subsection, the effect of 'string-moon' type extended branch radii (i.e., a_1 and a_2) is investigated. As a prerequisite, the remaining parameters were kept fixed.

Figures 8(a) and (b) depict the 3-dB ARBW of the antenna at resonant frequencies for the two patches at different radii. It is clear from the figures that when a_1 increases from 0 mm to 3 mm, the 3 dB-ARBW at 1.561 GHz increases from 161° to 222° and 195° to 211° at $\varphi = 0°$ and 90°, respectively; the 3-dB ARBW at 1.268 GHz increases and shows some fluctuations. As can be seen from the figure, when $a_1 = 2$ mm, the ARBW of both planes is the best.

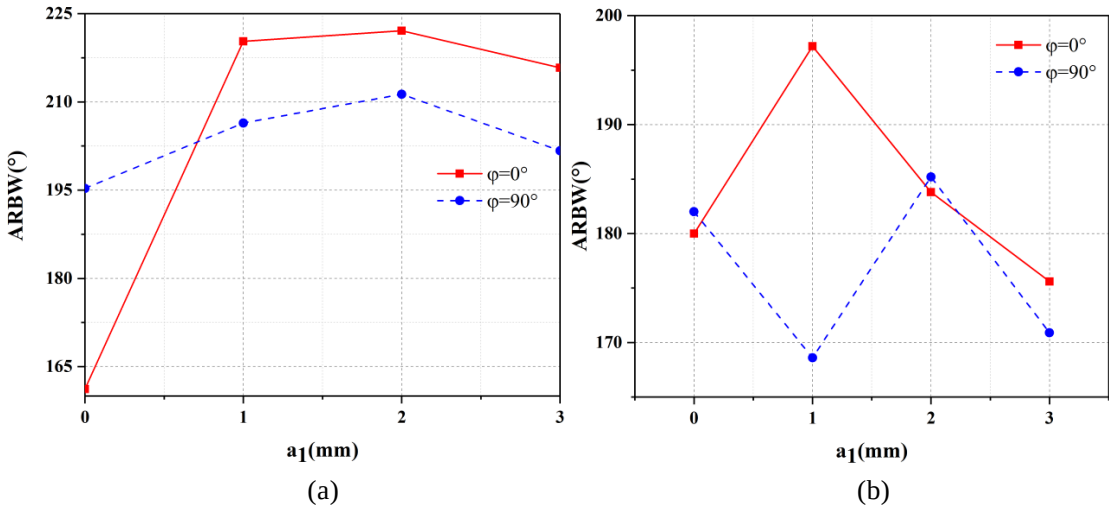

Figure 8. 3-dB ARBW of antenna with different values of a_1, (a) 3-dB ARBW at 1.561 GHz, (b) at 1.268 GHz.

Then, when a_1 is fixed to 2 mm, the 3-dB ARBW is calculated by simulating for different values of a_2 as shown in Figures 9(a) and (b).

As a_2 increases from 0 mm to 5 mm, the 3-dB ARBW at 1.561 GHz increases from 197° and 186° to 222° and 211° in the $\varphi = 0°$ and 90° planes, respectively, and the 3-dB ARBW at 1.268 GHz increases from 131° to 185° in the $\varphi = 0°$ plane, with fluctuations in the $\varphi = 90°$ plane. It can be seen from the figure that when $a_2 = 4$ mm, the 3-dB ARBW of the two planes reaches the best. Therefore, a_1 is chosen to be 2 mm, and a_2 is chosen to be 4 mm as a trade-off.

4.2. Effect of Radius of 30° Gap-Type APMS

In addition to the 'string-moon' type extended branch, APMS also has a significant effect on the electromagnetic wave diffraction, resulting in different radiative beam properties. In this section, the influence of APMS radius (i.e., r_1) on the 3-dB ARBW will be further studied when the 'string-moon' type extended branch radius is fixed at $a_1 = 2$ mm and $a_2 = 4$ mm.

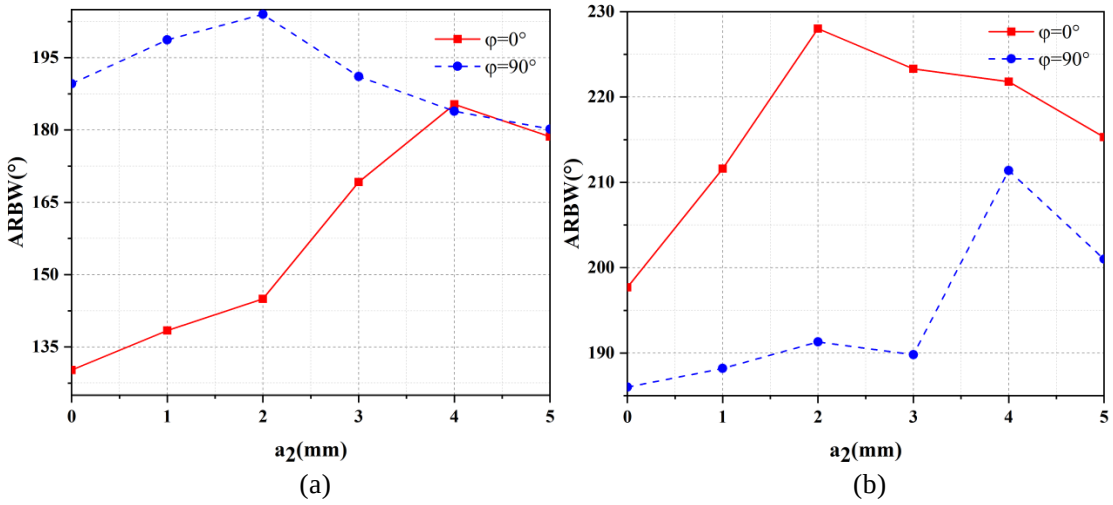

Figure 9. 3-dB ARBW of antenna with different values of a_2, (a) 3-dB ARBWs at 1.268 GHz, (b) at 1.561 GHz.

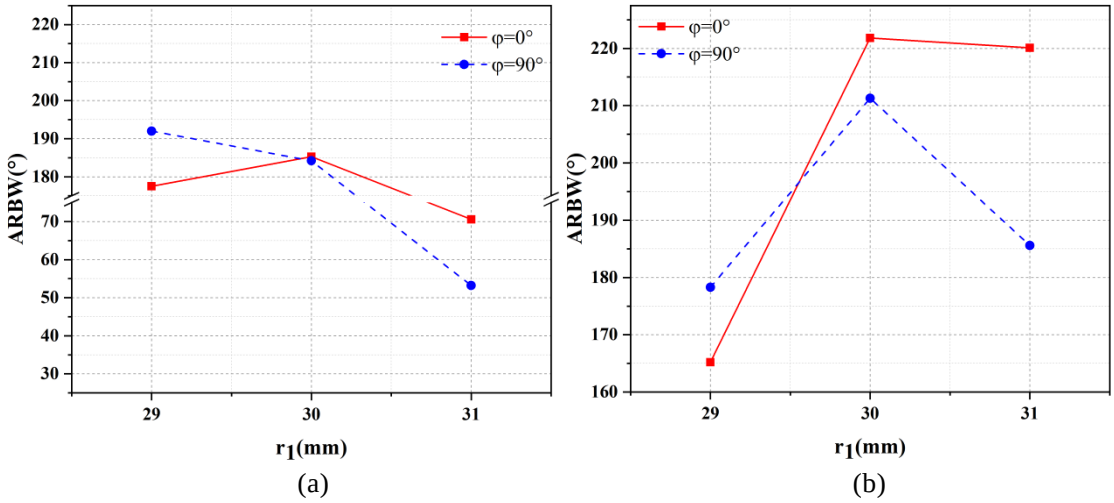

Figure 10. 3 dB-RBW of the antenna for different values of r_1 (a) at 1.268 GHz, (b) at 1.561 GHz.

As shown in Figure 10, when r_1 increases from 29 mm to 31 mm, the 3 dB-ARBW increases first and then decreases at both 1.561 GHz and 1.268 GHz at $\varphi = 0°$ and 90° planes, and reaches its maximum $r_1 = 30$ mm. At $r_1 = 30$ mm, the 3 dB-ARBWs at 1.561 GHz and 1.268 GHz are 222°, 211° and 185°, 184°, respectively.

5. RESULTS AND DISCUSSION

Electromagnetic simulation software is used to study and optimize the antenna structure, and the prototype of the proposed antenna is made and measured. $|S_{11}|$ was measured with a vector network analyzer, and the radiation pattern and AR were measured in an anechoic chamber.

As shown in Figure 11(a), it can be determined that there is a very good consistency between the simulations and measurements of the reflection coefficient ($|S_{11}|$). In the lower frequency band, the simulated S_{11} is below -10 dB between 1.25 and 1.33 GHz, and the measured range is between 1.25 GHz and 1.33 GHz. In the higher frequency bands, the simulated bandwidth range for 10 dB return loss is 1.52–1.59 GHz, and the measurement range has a bandwidth of 1.55 GHz to 1.63 GHz.

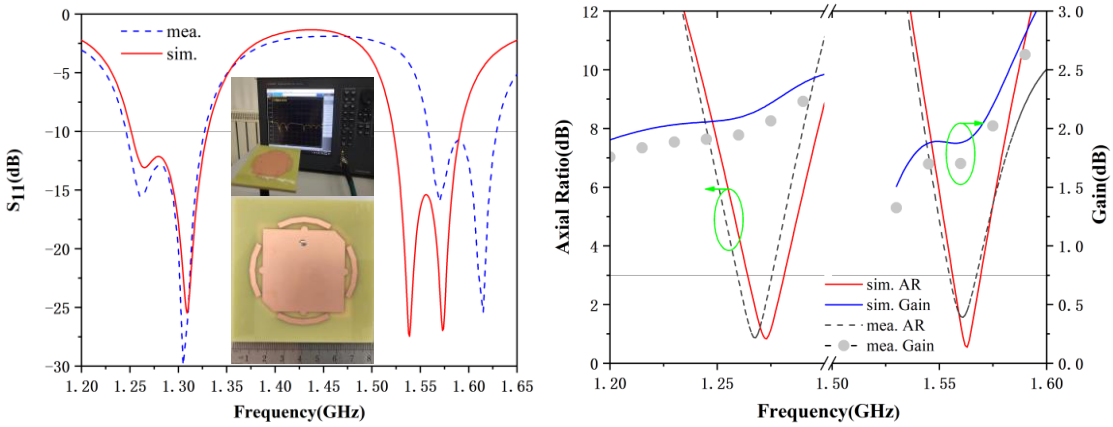

Figure 11. (a) Measurements and simulations were performed on the S_{11} of the prototype antenna. (b) Simulation and measurement of AR and gain of dual band.

In addition, the simulation and measurement of the AR are shown in Figure 11(b). In the lower frequency band, the simulated axis ratio bandwidth is 1.26–1.28 GHz, and the bandwidth of the measurement is 1.259–1.276 GHz. In the higher frequency band, the simulated bandwidth range is 1.55–1.57 GHz, and the measurement range has a bandwidth of 1.55–1.57 GHz for the axis ratio. Meanwhile, in the low frequency band, the measured and simulated peak gains are 2.15 dB and 2.00 dB, respectively, while in the high frequency band the values are 1.88 dB and 1.70 dB, respectively. The simulation results show that the simulated values are slightly higher because the losses in the feed cable and antenna fabrication are not considered in the simulation.

To further investigate the radiation performance of the antenna, the radiation patterns at both operating frequencies were also measured, and the results are shown in Figure 12. As can be seen from the figure, the simulated and measured radiation patterns at both operating frequencies are in good agreement.

Table 2. Comparison of the proposed antenna with the antenna in Ref.

Ref.	Single- or dual-band	Overall size (λ_0^3)	Fre. (GHz)	10-dB Bandwidth	3-dB AR bandwidth	Feed network	3-dB ARBW/°	
							$\varphi = 0°$	$\varphi = 90°$
[16]	Single	$\pi \times 0.132\times$ 0.132×0.064	1.2	20.8%	8.5%	Complex	190°	193°
[17]	Single	$0.368 \times 0.368\times$ 0.011	1.575	4%	1%	Simple	165°	176°
[18]	Dual	$\pi \times 0.368\times$ 0.368×0.105	1.228	N. A	0.65%	Simple	133°	135°
			1.575		0.83%		173°	170°
[19]	Single	0.21×0.21 $\times 0.016$	1.58	1.7%	0.63%	Simple	188°	188°
[20]	Dual	0.484×0.484	1.451	2.3%	0.62%	Simple	165°	182°
			2.029	3.1%	0.69%		175°	184°
[21]	Dual	0.475×0.475 $\times 0.03$	1.207	62.6%	7.1%	Complex	185°	187°
			1.561		9.6%		192°	194°
This Work	Dual	0.338×0.338 $\times 0.016$	1.268	6.3%	1.6%	Simple	185°	183°
			1.561	4.5%	1.2%		222°	210°

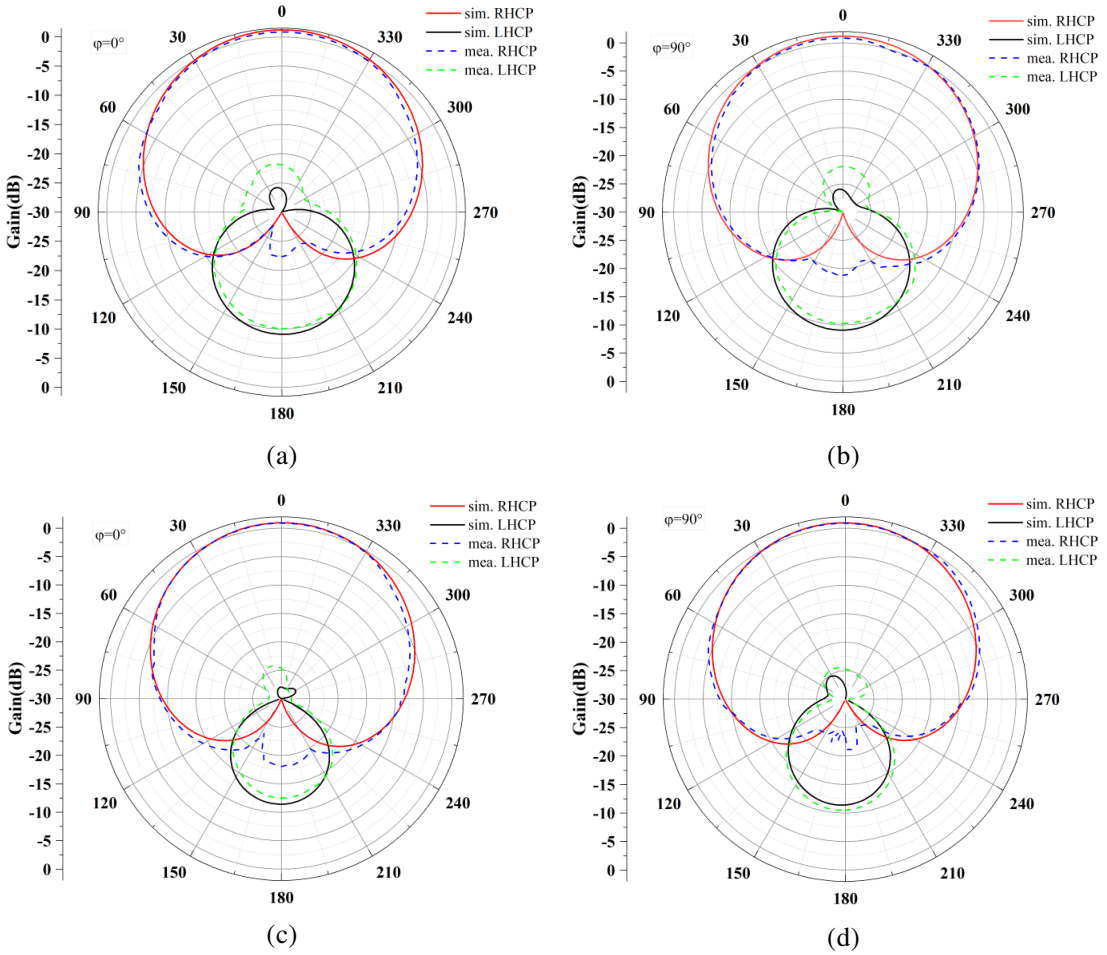

Figure 12. Simulation and measurement of radiation patterns in two main planes: (a) plane with $\varphi = 0°$ at 1.268 GHz; (b) plane with $\varphi = 90°$ at 1.268 GHz; (c) plane with $\varphi = 0°$ at 1.561 GHz; (d) plane with $\varphi = 90°$ at 1.561 GHz.

Table 2 summarizes the comparison of the performance among the proposed dual-band CP antenna and other reports. It can be clearly seen that the antenna can simultaneously realize dual-frequency operation, wide ARBW, and compact dimension through a simple feeding mode.

6. CONCLUSIONS

In this paper, a compact dual-band BDS antenna with wide 3-dB ARBW characteristics is proposed and analyzed. The 3-dB ARBW and axial ratio bandwidths of the proposed antenna are simultaneously broadened in both frequency bands with the proposed 'string moon' type branch extension technique. Furthermore, with 30° gap-type APMS, both frequency bands with a wider 3-dB ARBW of over 185° are further achieved. The experimental results show that the proposed CPMA is applicable to dual-frequency BDS applications and enhances the coverage angle of the systems.

REFERENCES

1. Zeng, D. Z. and Q. X. Chu, "Cavity-backed self-phased circularly polarized multidipole antenna with wide axial-ratio beamwidth," *IEEE Antennas Wireless Propag. Lett.*, Vol. 16, 1998–2001, 2017.

2. Wang, S. Y., X. Zhang, L. Zhu, and W. Wu, "Single-fed wide-beamwidth circularly polarized patch antenna using dual-function 3-D printed substrate," *IEEE Antennas Wireless Propag. Lett.*, Vol. 17, No. 4, 649–653, Apr. 2018.
3. Luo, Y., Q. X. Chu, and L. Zhu, "A low-profile wide-beamwidth circularly-polarized antenna via two pairs of parallel dipoles in a square contour," *IEEE Trans. Antennas Propag.*, Vol. 63, No. 3, 931–936, Mar. 2015.
4. Bai, X., J. Tang, X. Liang, J. Geng, and R. Jin, "Compact design of triple band circularly polarized quadrifilar helix antennas," *IEEE Antennas Wireless Propag. Lett.*, Vol. 13, 380–383, 2014.
5. Yang, Y.-H., J.-L. Guo, B.-H. Sun, and Y.-H. Huang, "Dual-band slot helix antenna for global positioning satellite applications," *IEEE Trans. Antennas Propag.*, Vol. 64, No. 12, 5146–5152, Dec. 2016.
6. Choi, E. C., J. W. Lee, and T. K. Lee, "Modified S-band satellite antenna with isoflux pattern and circularly polarized wide beamwidth," *IEEE Antennas Wireless Propag. Lett.*, Vol. 12, 1319–1322, 2013.
7. Tang, C. L., J. Y. Chiou, and K. L. Wong, "Beamwidth enhancement of a circularly polarized microstrip antenna mounted on a three-dimensional ground structure," *Microw. Opt. Technol. Lett.*, Vol. 32, No. 2, 149–153, Jan. 2002.
8. Su, C. W., S. K. Huang, and C. H. Lee, "CP microstrip antenna with wide beamwidth for GPS band application," *Electron. Lett.*, Vol. 43, No. 20, 1062–1063, Sep. 2007.
9. Bao, X. L. and M. J. Ammann, "A cavity-backed spiral slot antenna with wide axial ratio beamwidth for GPS system," *Microw. Opt. Technol. Lett.*, Vol. 56, No. 5, 1050–1054, May 2014.
10. Son, H. W., H. Park, K. H. Lee, G. J. Jin, and M. K. Oh, "UHF RFID reader antenna with a wide beamwidth and high return loss," *IEEE Trans. Antennas Propag.*, Vol. 60, No. 10, 4928–4932, Oct. 2012.
11. Liu, N. W., L. Zhu, and W. W. Choi, "Low-profile wide-beamwidth circularly-polarised patch antenna on a suspended substrate," *IET Microw. Antennas Propag.*, Vol. 10, No. 8, 885–890, May 2016.
12. Zhang, X., L. Zhu, and N. W. Liu, "Pin-loaded circularly-polarized patch antennas with wide 3-dB axial ratio beamwidth," *IEEE Trans. Antennas Propag.*, Vol. 65, No. 2, 521–528, Feb. 2017.
13. Zhang, X., L. Zhu, N. W. Liu, and D. P. Xie, "Pin-loaded circularly-polarized patch antenna with sharpened gain roll-off rate and widened 3-dB axial ratio beamwidth," *IET Microw. Antennas Propag.*, Vol. 12, No. 8, 1247–1254, 2018.
14. Lee, S. K., A. Sambell, E. Korolkiewicz, S. F. Ooi, and Y. Qin, "Design of a circular polarized nearly square microstrip patch antenna with offset feed," *High Frequency Postgraduate Student Colloquium*, Vol. 2004, 61–66, 2004, doi: 10.1109/HFPSC.2004.1360353.
15. Zhai, J., G. Chen, W. Wang, Y. Liu, L. Wang, and Z. Wang, "A novel low profile circularly polarized GNSS antenna with wide 3 dB axial ratio beamwidth," *Progress In Electromagnetics Research M*, Vol. 111, 199–208, 2022.
16. Chen, X., D. Wu, L. Yang, and G. Fu, "Compact circularly polarized microstrip antenna with cross-polarization suppression at low-elevation angle," *IEEE Antennas Wireless Propag. Lett.*, Vol. 16, 258–261, May 2017.
17. Xie, L. J., Y. Y. Li, and Y. C. Zheng, "A wide axial-ratio beamwidth circularly polarized microstrip antenna," *2016 IEEE International Conference on Ubiquitous Wireless Broadband (ICUWB)*, 1–4, Dec. 2016.
18. Zhong, Z.-P., et al., "A compact dual-band circularly polarized antenna with wide axial-ratio beamwidth for vehicle GPS satellite navigation application," *IEEE Transactions on Vehicular Technology*, Vol. 68, No. 9, 8683–8692, Sept. 2019, doi: 10.1109/TVT.2019.2920520.
19. Wang, M.-S., X.-Q. Zhu, Y.-X. Guo, and W. Wu, "Compact circularly polarized patch antenna with wide axial ratio beamwidth," *IEEE Antennas Wireless Propag. Lett.*, Vol. 17, No. 4, 714–718, Apr. 2018.

20. Bao, X. L. and M. J. Ammann, "Dual-frequency dual circularly-polarised patch antenna with wide beamwidth," *Electron. Lett.*, Vol. 44, No. 21, 1233–1234, Oct. 2008.
21. Liu, H., C. Xun, S.-J. Fang, and Z. Wang, "Compact dual-band circularly polarized patch antenna with wide 3-dB axial ratio beamwidth for Beidou applications," *Progress In Electromagnetics Research M*, Vol. 87, 103–113, 2019.